# Predicting 3D-printed concrete process parameters through Discrete Element Modeling

Victor Hugo M. Avancini[1], Osvaldo D. Quintana-Ruiz[2], Eduardo M. B. Campello[1]

[1]*Dept. of Structural and Geotechnical Engineering, Polytechnic School, University of São Paulo (USP)*
[2] *Computational Mechanics Laboratory, Faculty of Engineering, National University of Asunción, Campus de la UNA, San Lorenzo, Paraguay*
*P.O. Box 61548, 05424-970, SP/São Paulo, Brazil*
*victor.avancini@usp.br, oquintana@ing.una.py, campello@usp.br*

**Abstract.** Three-dimensional concrete printing (3DCP) has emerged as a promising manufacturing technique in the civil engineering sector, offering myriad advantages over traditional construction methods. Despite its potential, challenges persist in optimizing the manufacturing stage of 3DCP, including determining optimal fresh concrete rheology, layer thickness, print path, and nozzle characteristics. In this study, we incorporate the Discrete Fresh Concrete model (DFC) into our Discrete Element Method (DEM) code to simulate the rheological behavior of fresh printable concrete during printing, aiming to explore a comprehensive range of process parameters and their combinations to enhance understanding and optimization 3DCP process. Through a series of simulations, we systematically vary some of the process variables such as concrete mix design, nozzle specifications, and printing speed to investigate their influence on the printed output quality. By the obtained results, we aim to identify the key parameters that significantly affect the process, offering insights for refining 3DCP technologies and helping guide their development. We believe methodologies of the type shown here may be an efficient tool for advancing 3DCP technologies.

**Keywords:** 3D concrete printing, particles, discrete element methods (DEM)

## 1 Introduction

Additive manufacturing, or 3D printing, has recently become a revolutionary technology with broad applications. One recent application of additive manufacturing is in civil construction, offering numerous advantages over traditional methods. By automating manual processes, concrete 3D printing enhances efficiency and allows for complex structures that are difficult or impossible to create manually, reducing errors and rework. It also promotes sustainability by using materials more efficiently and reducing waste, with the added benefit of incorporating sustainable or recycled materials to reduce environmental impact. Additionally, 3D printing significantly reduces construction time as it operates continuously, accelerating project completion and lowering operational costs. The precision of 3D printing ensures effective material use, resulting in substantial material savings. Finally, 3D printing provides almost unlimited flexibility in architectural design, enabling the creation of complex geometries that are customized to specific project needs. However, there are still some uncertainties and technological challenges that need to be addressed before 3DCP can be widely adopted in the construction industry, including: (i) current 3D printing technologies require improved materials in order to reach their full potential; (ii) concrete rheological characteristics need to be considered when developing new 3D printing technologies; and (iii) the required pumping and extrusion pressure during the 3DCP process.

To address the challenges associated with 3DCP, numerical simulation may be an effective tool. Considering that fresh concrete has a rather discrete (and two-phase) nature at the level of coarse aggregates, the discrete element method (DEM) stands as a natural approach. First introduced by Cundall in the 1970s [1, 2] and further refined by Cundall and Strack [3], DEM can be understood as a model for the representation and study of granular

materials. It proposes numerically solving the differential equations of motion for systems composed of a large number of rigid solids ("discrete elements" or "particles") [4]. In DEM simulations, these individual particles are treated as discrete entities, and their interactions are governed by simple mechanical laws, such as contact forces, frictional forces, and others. By tracking the motion of each (and all) individual particles and considering their interactions, DEM provides valuable insights into complex phenomena at any desired time instant. This includes individual particle trajectories, forces interacting, interactions among neighboring particles, and many other factors that are challenging to obtain through experimental techniques.

This article presents an approach that combines the DEM formulation for modeling particle dynamics with the DFC model equations to account for particle-particle and particle-wall interactions in fresh printable concrete. The DFC model, introduced by Cusatis and Ramyar [5], is based on stress-strain relationships to represent the contact interactions, and, when used in the DEM framework, provides an accurate description of the interactions among coarse aggregate particles within a fine mortar matrix. They idealize each particle as spheres with two phases: (i) a rigid inner sphere (representing the aggregate) and (ii) a soft outer layer, covering the first (representing the mortar), with a known thickness. Our approach adopts the DEM formulation developed by Campello [4, 6, 7] and Quintana-Ruiz and Campello [8] for the mechanical part of the problem.

## 2 Methodology

In this work we incorporate the DFC model, developed by Cusatis and Ramyar [5], to describe contact between particles (and between particle and wall) in our in-house DEM code. Our main objective is to simulate the rheological behavior of fresh concrete for 3D concrete printing.

### 2.1 Particle's Dynamics

In this study, we adopt a Lagrangian DEM description. Let us consider a system of $N_P$ spherical "biphasic" particles, consisting of a rigid inner sphere covered by a thin layer of soft mortar on the outside, each characterized with essential properties, including mass $m_i$, radius $R_i$, aggregate radius $r_i$, mortar thickness $h_i$ (Fig. 1) and rotation inertia $j_i$ (relative to particle's center). To mathematically describe their motion, we represent the position vector of each particle as $\boldsymbol{x}_i$, the velocity vector as $\boldsymbol{v}_i$, the incremental rotation vector as $\boldsymbol{\alpha}_i^{\Delta}$ (rotation vector relative to two consecutive configurations) and the spin vector as $\boldsymbol{\omega}_i$. Following classical dynamics (Newton-Euler), the equations of motion for the $i$th particle are

$$\begin{aligned} m_i\dot{\boldsymbol{v}}_i &= \boldsymbol{f}_i^{con} + \boldsymbol{f}_i^{env}, \\ j_i\dot{\boldsymbol{\omega}}_i &= \boldsymbol{m}_i^{con}, \end{aligned} \tag{1}$$

where $\boldsymbol{f}_i^{con}$ are the forces due to mechanical contacts with other particles or walls and $\boldsymbol{f}_i^{env}$ are the forces due to the environment (in this study, we take only the gravitational contribution $m_i\boldsymbol{g}$, where $\boldsymbol{g}$ is the gravity acceleration vector). Still in eq. (1), $\boldsymbol{m}_i^{con}$ are the moments induced by the contact forces and $j_i$ is usually a matrix called inertia moment of the particle $i$ around its axis of rotation. The moment of inertia represents the resistance of the particle to changes in its rotation motion. For a solid, homogeneus sphere of mass $m$ and radius $R$, the moment of inertia is given by:

$$j_i = \frac{2}{5}mR^2. \tag{2}$$

It is important to mention that there are works in the literature that incorporate additional forces into the model, such as adhesive and drag forces, among others [4, 6–8]. Mechanical contacts forces acting on a particle $i$ due to contact with $N_i^c$ other particles or walls, $\boldsymbol{f}_i^{con}$, include both the normal component $\boldsymbol{f}_i^{con,n}$ and the tangential component $\boldsymbol{f}_i^{con,t}$ (i.e., friction forces), given by 3.

$$\begin{aligned} \boldsymbol{f}_i^{con} &= \sum_{j=1}^{N_i^c}(\boldsymbol{f}_{ij}^{con,n} + \boldsymbol{f}_{ij}^{con,t}) \\ \boldsymbol{f}_{ij}^{con,n} = -\frac{4}{3}\sqrt{r^*}E^*\delta_{ij}^{3/2}\boldsymbol{n}_{ij} - d^{con,n}\dot{\delta}_{ij}\boldsymbol{n}_{ij}, &\qquad \boldsymbol{f}_{ij}^{con,t} = -(k^{con,t}\Delta\boldsymbol{x}_{ij}^{trial} + d^{con,t}\boldsymbol{v}_{ij}), \end{aligned} \tag{3}$$

where

$$r^* = \frac{r_i r_j}{r_i + r_j} \qquad E^* = \frac{E_i E_j}{E_j(1-\nu_i^2) + E_i(1-\nu_j^2)} \qquad \boldsymbol{n}_{ij} = \frac{\boldsymbol{x}_j - \boldsymbol{x}_i}{||\boldsymbol{x}_j - \boldsymbol{x}_i||}, \tag{4}$$

where $r^*$ and $E^*$ are the effective radius and effective elasticity modulus of particle pair $i-j$ (with $E_i$ and $\nu_i$ the elasticity modulus and Poisson coefficient of particle $i$ and the $E_j$ and $\nu_j$ the elasticity modulus and Poisson coefficient of particle $j$), respectively; $\boldsymbol{n}_{ij}$ is the unit vector that points from the center of particle $i$ to center of particle $j$; and $\dot{\delta}_{ij}$ is the overlap velocity of the pair. Still in eq. (3), $\delta_{ij}$ is the overlap between particles and $d^{con,n}$ is the damping constant, which are given by

$$\begin{gathered} \delta_{ij} = ||\boldsymbol{x}_i - \boldsymbol{x}_j|| - r_i + r_j, \\ d^{\text{con,n}} = 2\xi^{\text{con,n}}\sqrt{2E^* m^* \sqrt{r^*}\delta_{ij}^{1/4}} \qquad \text{with} \qquad m^* = \frac{m_i m_j}{m_i + m_j}, \end{gathered} \tag{5}$$

where $\xi^{\text{con,n}}$ is the damping rate and $m^*$ is the effective mass of pair $i-j$. For the tangential components $\boldsymbol{f}_i^{con,t}$, we determined them through trials following the Coulomb model. In 3, $k^{con,t}$ is the spring stiffness, $d^{con,t}$ is the damping constant of the tangential force, $\Delta\boldsymbol{x}_{ij}^{trial}$ is the trial tangential elongation, and $\boldsymbol{v}_{ij}$ is the elongation velocity.

Friction forces are not central forces, meaning they have an eccentricity relative to the centers of mass of the particles on which they act. Consequently, these particles undergo rotational motion, which affects their overall movement. The resultant of the moments due to the friction forces acting on a particle $i$, resulting from contacts with $n_i^{con}$ other particles, is given by

$$\boldsymbol{m}_i^{fric} = \sum_{j=1}^{n_i^{con}} \boldsymbol{m}_{ij}^{fric} \qquad \text{with} \qquad \boldsymbol{m}_{ij}^{fric} = \boldsymbol{r}_i^P \times \boldsymbol{f}_{ij}^{con,t}, \tag{6}$$

where $m_{ij}^{fric}$ is the moment induced in a particle $i$ due to the friction force with another particle $j$, and $\boldsymbol{r}^P$ is the vector connecting the center of particle $i$ with the contact point $P$.

This section shows how the conventional DEM works (for more details, see Campello [4, 6, 7] and Quintana-Ruiz and Campello [8]). For modeling the fresh concrete past the contact model from eq. (3) to eq. (6) will be replaced by a model based on constitutive equations, which is the Discrete Fresh Concrete (DFC).

### 2.2 Discrete Fresh Concrete (DFC)

The DFC model uses DEM principles with stress-strain relationships to more accurately represent the behavior of fresh concrete. The model represents each particle as a biphasic element, consisting of a rigid inner sphere with radius $r_i$ representing the aggregate, and a thin outer soft layer $h_i$ representingthe mortar (see Fig. 1a) . Thus, the contact between two particles can be: (i) mortar-mortar, when the distance between their centers is greater than the so-called equilibrium configuration ($L_{ij0} = r_i + r_j + h_i$); (ii) mortar-aggregate, when the distance between the centers is less than $L_{ij0}$ but greater than the sum of the aggregate radii $r_i$ and $r_j$; (iii) aggregate-aggregate, when the distance between the centers is equal to or less than the sum of the aggregate radii.

Specifically, the model is designed to accurately represent mortar-to-mortar contact, i.e., between the outer layers of each particle. As a result, the equations of motion (eq. (1)) for the $i$th particle can be reformulated as

$$m_i\dot{\boldsymbol{v}}_i = \boldsymbol{f}_i^{dfc} + \boldsymbol{f}_i^{env} \qquad j_i\dot{\boldsymbol{\omega}}_i = \boldsymbol{m}_i^{dfc}, \tag{7}$$

where $\boldsymbol{f}_i^{dfc}$ are the forces on particle $i$ due to mechanical contact with other particles (or between particle and wall), $\boldsymbol{f}_i^{env}$ are the forces on particle $i$ due to the environment that may arise from the possible existence of gravitational, electric and/or magnetic fields, $\boldsymbol{m}_i^{dfc}$ are the moments on particle $i$ induced by other particles or walls. The calculation of the forces and moments acting on the particle due to its interactions with other particles and walls are

$$\boldsymbol{f}_i^{dfc} = \sum_j A_{ij}\boldsymbol{\sigma}_{ij} \qquad \boldsymbol{m}_i^{dfc} = \sum_j A_{ij}(\boldsymbol{a}_i \times \boldsymbol{\sigma}_{ij}) \tag{8}$$

where $\boldsymbol{\sigma}_{ij}$ is the contact stress on particle $i$ at the contact point with particle $j$ and $\boldsymbol{a_i}$ is the vector from the center of particle $i$ to the contact area center, $A_{ij}$ in Fig. 1b. The contact area $A_{ij}$ is given by $A_{ij} = \pi(H_{ij})^2$.

Given that particles are spherical, the contact area formed between two particles or between a particle and a wall can be modeled as a circle with radius $H_{ij}$, which is calculated from sheer geometrical arguments as follows:

$$H_{ij} = \sqrt{(R_i)^2 - (a_i)^2} \qquad \text{and} \qquad a_i = \frac{(R_i)^2 - (R_j)^2 + (L_{ij})^2}{2L_{ij}}, \tag{9}$$

where $a_i$ is the distance from the center of particle $i$ to the contact area center and $L_{ij}$ is the distance between the center of particle $i$ and $j$ (or object) and can be calculates as $L_{ij} = ||\boldsymbol{x}_j - \boldsymbol{x}_i||$.

Still in eq. (8), to calculate $\boldsymbol{\sigma}_{ij}$ and $\boldsymbol{a_i}$, it is necessary to establish a local Cartesian reference system, Fig. 1c. This reference system is based on the motion of particles $i$ and $j$ according to the classical Lagrangian formulation. The unit vector $\boldsymbol{e}_{\boldsymbol{N}}^{ij}$ is oriented along the line segment connecting the center of the two particles, which is calculated as follows:

$$\boldsymbol{e}_{\boldsymbol{N}}^{ij} = \frac{\boldsymbol{x}_j - \boldsymbol{x}_i}{L_{ij}}. \tag{10}$$

To fully establish the local Cartesian reference system, the unit vector $\boldsymbol{e}_{\boldsymbol{M}}^{ij}$ is calculated using the direction of the relative tangential velocity between the particle $i$ and $j$ (or object) at the point of contact $\boldsymbol{v}_{rel,t}^P$, and the unit vector $\boldsymbol{e}_{\boldsymbol{L}}^{ij}$, in turn, is oriented as to form a right-handed coordinate system. The unit vectors $\boldsymbol{e}_{\boldsymbol{M}}^{ij}$ and $\boldsymbol{e}_{\boldsymbol{L}}^{ij}$ are given by

$$\boldsymbol{e}_{\boldsymbol{M}}^{ij} = ||\boldsymbol{v}_{rel,t}^P - (\boldsymbol{v}_{rel,t}^P \cdot \boldsymbol{e}_{\boldsymbol{N}}^{ij})\boldsymbol{e}_{\boldsymbol{N}}^{ij}||, \qquad \boldsymbol{e}_{\boldsymbol{L}}^{ij} = \boldsymbol{e}_{\boldsymbol{N}}^{ij} \times \boldsymbol{e}_{\boldsymbol{M}}^{ij}. \tag{11}$$

where, $\boldsymbol{v}_{rel,t}^P$ is calculated from the relative velocity at contact point $\boldsymbol{v}_{rel}^P$, which are given by

$$\boldsymbol{v}_{rel,t}^P = \boldsymbol{v}_{rel}^P - (\boldsymbol{v}_{rel}^P \cdot \boldsymbol{e}_{\boldsymbol{N}}^{ij})\boldsymbol{e}_{\boldsymbol{N}}^{ij}, \qquad \boldsymbol{v}_{rel}^P = \boldsymbol{v}_j + \boldsymbol{\omega}_j \times \boldsymbol{a}_j - \boldsymbol{v}_i + \boldsymbol{\omega}_i \times \boldsymbol{a}_i, \tag{12}$$

Given the distance $a_i$, the vector $\boldsymbol{a_i}$ is calculated as $\boldsymbol{a}_i = a_i \boldsymbol{e}_N^{ij}$.

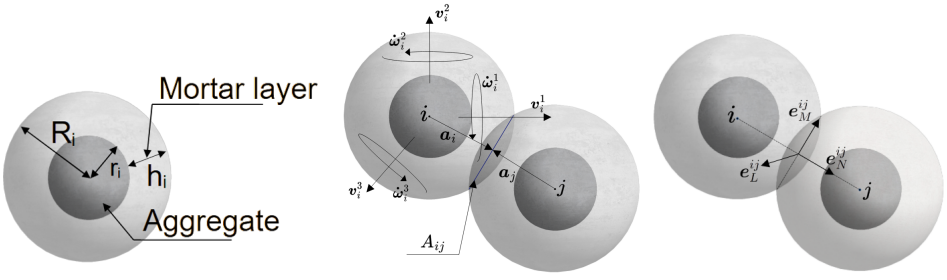


(a) (b) (c)

Figure 1. (a) representation of a generic particle in the DFC model (b) general configuration of two interacting particle; (c) local Cartesian reference system

In the DFC model, $\boldsymbol{\sigma}_{ij}$ is the sum of a stiffness stresses $\boldsymbol{\sigma}_s$ with a viscous stresses $\boldsymbol{\sigma}_v$, which are given by

$$\boldsymbol{\sigma}_{ij} = \boldsymbol{\sigma}_s + \boldsymbol{\sigma}_v \qquad \text{with,} \qquad \boldsymbol{\sigma}_s = \begin{bmatrix} \sigma_{Ns} \\ \sigma_{Ms} \\ \sigma_{Ls} \end{bmatrix} \qquad \text{and} \qquad \boldsymbol{\sigma}_v = \begin{bmatrix} \sigma_{Nv} \\ \sigma_{Mv} \\ \sigma_{Lv} \end{bmatrix} \tag{13}$$

where, to calculate $\boldsymbol{\sigma}_s$ and $\boldsymbol{\sigma}_v$ we consider the current configuration of the particle pair, which is defined by the relative position between them. In a generic configuration (Fig. 1a), the contact between two particles begins when $L_{ij} < r_i + r_j + 2h$ and the equilibrium is configured when $L_{ij} = L_{ij0} = r_i + r_j + h$, where $h$ is the mortar layer. Which means that, when two particles are in contact and $L_{ij} > L_{ij0}$, they are in tension (and we called it soft contact) and this is the case when particles are with attractive forces. Similarly, when $L_{ij} < L_{ij0}$ and $L_{ij} > r_i + r_j$, compression appears (also called it soft contact), causing repulsive forces. In addition, when $L_{ij} = L_{ij0}$, we are in zero (or neutral) configuration, and then no force is applied. Finally, when $L_{ij} = r_i + r_j$, the aggregates of particles $i$ and $j$ are in contact (and we called it hard contact). When in tension ($L_{ij} > L_{ij0}$) or compression, i.e. soft contact, ($L_{ij} < L_{ij0}$ and $L_{ij} > r_i + r_j$), $\boldsymbol{\sigma_s}$ and $\boldsymbol{\sigma_v}$ are

$$\boldsymbol{\sigma_s} = \begin{bmatrix} E_{Nm}\varepsilon_N^{ij} \\ 0 \\ 0 \end{bmatrix} \qquad \boldsymbol{\sigma_v} = \begin{bmatrix} \beta\eta(\dot{\gamma})\dot{\varepsilon}_N^{ij} \\ \eta(\dot{\gamma})\dot{\varepsilon}_M^{ij} \\ \eta(\dot{\gamma})\dot{\varepsilon}_L^{ij} \end{bmatrix}, \tag{14}$$

otherwise, when hard contact develops, i.e. $L_{ij} = r_i + r_j$, $\boldsymbol{\sigma_s}$ and $\boldsymbol{\sigma_v}$ are

$$\boldsymbol{\sigma_s} = \begin{bmatrix} E_{Na}\varepsilon_N^{ij} \\ \alpha_a E_{Na}\varepsilon_M^{ij} \\ \alpha_a E_{Na}\varepsilon_L^{ij} \end{bmatrix} \qquad \boldsymbol{\sigma_v} = \begin{bmatrix} \beta\eta(\dot{\gamma})\dot{\varepsilon}_N^{ij} \\ \eta(\dot{\gamma})\dot{\varepsilon}_M^{ij} \\ \eta(\dot{\gamma})\dot{\varepsilon}_L^{ij} \end{bmatrix}, \tag{15}$$

where $E_{Nm}$ is the mortar normal elastic modulus, $E_{Na}$ is the aggregate normal elastic modulus, $\alpha_a$ is the normal-shear coupling parameter and

$$\dot{\varepsilon}_N^{ij} = \frac{\boldsymbol{v}_{\text{rel}}^P \cdot \boldsymbol{e}_N^{ij}}{L_{ij}}, \qquad \dot{\varepsilon}_M^{ij} = \frac{\boldsymbol{v}_{\text{rel}}^P \cdot \boldsymbol{e}_M^{ij}}{L_{ij}}, \qquad \dot{\varepsilon}_L^{ij} = \frac{\boldsymbol{v}_{\text{rel}}^P \cdot \boldsymbol{e}_L^{ij}}{L_{ij}}, \tag{16}$$

are the strain rates in directions N, M and L. Still in eq. (14) and eq. (15), $\eta(\dot{\gamma})$ is the mortar's apparent viscosity, which is given by

$$\begin{aligned} \eta(\dot{\gamma}) &= \eta_0 = \kappa_0\eta_\infty \quad \text{if} \quad \dot{\gamma} \leq \dot{\gamma}_0 \\ \eta(\dot{\gamma}) &= \eta_\infty|\dot{\gamma}|^{n-1} \quad \text{if} \quad \dot{\gamma}_0 < \dot{\gamma} \end{aligned} \tag{17}$$

and

$$\dot{\gamma} = \sqrt{\beta\dot{\varepsilon}_N^2 + \dot{\varepsilon}_M^2 + \dot{\varepsilon}_L^2} \quad \text{and} \quad \dot{\gamma}_0 = \sigma_{\tau 0}/\eta_0 \tag{18}$$

where $\sigma_{\tau 0}$ is the shear yield stress, $\kappa_0 = 100$ is a penalty constant, $\eta_\infty$ is the mortar plastic viscosity and $n$ refers to Newtonian ($n = 1$), shear-thickening ($n > 1$), and shear-thinning ($n < 1$) flow.

The interaction between particle and surfaces, considers any surface as padded and characterized by a thickness $p$. The interaction between particle and surface is identical to the particle-particle model. The differences in this case are: (i) the center to center distance $L_{ij}$ is replaced by the shortest distance between particle and surface; (ii) the zero-configuration becomes $L_0 = r_i + h/2 + p$; and (iii) the distance of particle $i$ from the center of contact area becomes $a_i = L_{ij} - p$. For more comprehensive details of the DFC formulation, readers may refer to (Cusatis and Ramyar) [5].

## 3 Numerical Solution Scheme

To solve the mechanical problem, we integrate the governing equations (eq. (8)) numerically by means of an explicit (forward Euler) scheme. We obtain the values of position, velocity, spin and incremental rotations at time $t_{i+1}$ based on the known values at time $t_i$. Then we increment the time by $\Delta t$ and transfer the information

from $i+1$ to $i$ ($i \leftarrow i+1$). Subsequently, the procedure is repeated until the final simulation time $t_F$ is reached. The eq. (19), eq. (20), eq. (21) and eq. (22) represent the calculation of the particle's velocity, spin, position, and incremental rotation at time $t_{i+1}$, respectively.

$$\boldsymbol{v_i}(t+\Delta t) = \boldsymbol{v_i}(t) + \frac{1}{m_i}\int_t^{t+\Delta t}(\boldsymbol{f}_i^{dfc} + \boldsymbol{f}_i^{env})dt \approx \boldsymbol{v}_i(t) + \frac{\Delta t}{m_i}[\boldsymbol{f}_i^{dfc}(t) + \boldsymbol{f}_i^{env}(t)], \tag{19}$$

$$\boldsymbol{\omega_i}(t+\Delta t) = \boldsymbol{\omega_i}(t) + \frac{1}{j_i}\int_t^{t+\Delta t}(\boldsymbol{m}_i^{dfc})dt \approx \boldsymbol{\omega_i}(t) + \frac{\Delta t}{j_i}[\boldsymbol{m}_i^{dfc}(t)], \tag{20}$$

$$\boldsymbol{x}_i(t+\Delta t) = \boldsymbol{x}_i(t) + \boldsymbol{v}_i(t+\Delta t)\Delta t, \tag{21}$$

$$\boldsymbol{\alpha}_i^{\Delta}(t+\Delta t) = \boldsymbol{\omega}_i(t+\Delta t)\Delta t. \tag{22}$$

The solution process can be schematically seen in the following algorithm:

**Solution Algorithm**

Step 1 Initialize time variables and get initial conditions:

$t = 0$, $\Delta t =$ given

$\boldsymbol{x}_i(0)$, $\boldsymbol{v}_i(0)$, $\boldsymbol{\omega}_i(0)$, $\boldsymbol{\alpha}_i(0)$ = given $\quad (i = 1, \ldots, N_p)$

Step 2 **While** $t \leq t_{\text{final}}$, loop over all particles: **For** $i = 1, \ldots, N_p$ **Do**

Compute forces and moments at time $t$ via eq. (8)

Update velocity, spin, position, and incremental rotation vectors:

$\boldsymbol{v_i}(t+\Delta t) = \boldsymbol{v}_i(t) + \frac{\Delta t}{m_i}[\boldsymbol{f}_i^{dfc}(t) + \boldsymbol{f}_i^{env}(t)]$,

$\boldsymbol{\omega_i}(t+\Delta t) = \boldsymbol{\omega_i}(t) + \frac{\Delta t}{j_i}[\boldsymbol{m}_i^{dfc}(t)]$,

$\boldsymbol{x}_i(t+\Delta t) = \boldsymbol{x}_i(t) + \boldsymbol{v}_i(t+\Delta t)\Delta t$,

$\boldsymbol{\alpha}_i^{\Delta}(t+\Delta t) = \boldsymbol{\omega}_i(t+\Delta t)\Delta t$

Save updated variables:

$\boldsymbol{v_i}(t) \leftarrow \boldsymbol{v_i}(t+\Delta t)$,

$\boldsymbol{\omega_i}(t) \leftarrow \boldsymbol{\omega_i}(t+\Delta t)$,

$\boldsymbol{x_i}(t) \leftarrow \boldsymbol{x_i}(t+\Delta t)$,

$\boldsymbol{\alpha_i}(t) \leftarrow \boldsymbol{\alpha_i}(t+\Delta t)$,

$t \leftarrow t + \Delta t$

**End do**

## 4 Results

To investigate the ability of the DFC model to simulate a 3D printing process, Figure 2a presents the attempts to print with varying printing speeds. In all simulations, the average radius of the aggregates is $r = 2mm$ and the mortar thickness is $h = 1mm$, with $E_{Nm} = 50KPa$, $N_\infty = 50Pa.s$, and $\sigma_{\tau 0} = 500Pa$. The nozzle featured a rectangular cross-section with dimensions of $30 \times 15mm$, and simulations were conducted with nozzle speeds ranging from 6 to 20 cm/s, deposition speed with 7 cm/s and $\Delta t = 2 \times 10^{-5}$ . As shown in Figure 2b, when nozzle speed are 6 and 8 cm/s, the deposition is quite consistent and has good resolution. However, at higher speeds, we observe filament rupture, which becomes progressively more pronounced as the nozzle speed increases.

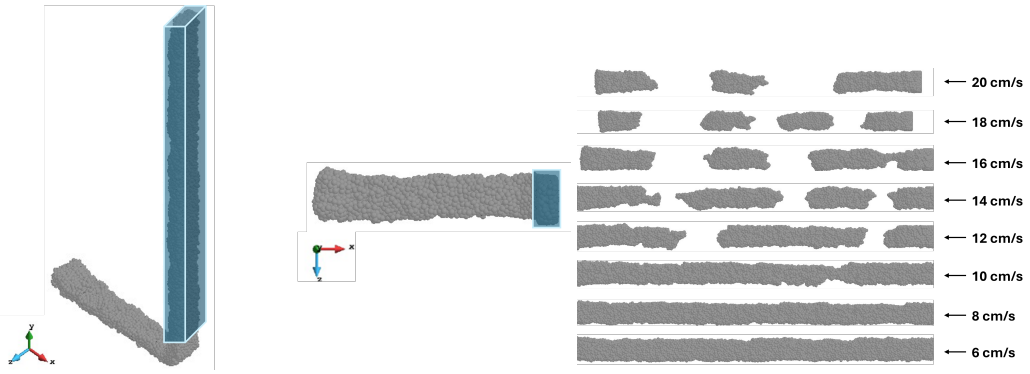


(a) (b)

Figure 2. (a) 3D concrete printing. (b) 3D concrete printing with varying nozzle speed

## 5 Conclusions

In conclusion, this work presents an approach that combines the Discrete Element Method (DEM) with the DFC model for modelling fresh printable concrete, in an attempt to simulate 3D Concrete Printing (3DCP). The DFC model can be considered a useful numerical tool for modeling printable concrete deposition, as it can be used to simulate the printability of concrete in an additive manufacturing process. The computational implementation of the model is fairly straightforward and enables a quick simulation tool for qualitative process design and analysis. We believe it can be beneficial for engineers and analysts in the field, helping to evaluate the overall process response under varying parameters. General trends can be identified, and what-if scenarios can be explored at a reasonable computational cost and model complexity. New simulations are underway, considering the printing of multiple layers and more complex geometric shapes.

**Acknowledgements.** First author acknowledges support by CAPES (Coordenação de Aperfeiçoamento de Pessoal de Nível Superior) Brazil. The third author acknowledges support from CNPq (Conselho Nacional de Desenvolvimento Científico e Tecnológico), Brazil, under grant 313046/2021-2.

**Authorship statement.** The authors hereby confirm that they are the sole liable persons responsible for the authorship of this work, and that all material that has been herein included as part of the present paper is either the property (and authorship) of the authors, or has the permission of the owners to be included here.

## References

[1] P. A. Cundall. A computer model for simulating progressive, large-scale movements in blocky rock systems. *Proc. Symp. Int. Soc. Rock Mech*, vol. , 1971.
[2] P. A. Cundall. A computer model for rock-mass behavior using interactive graphics for the input and output of geometrical data. *Report MRD-2-74. University of Minnesota (for Missouri River Division, US Army Corps of Engineers)*, vol. , 1974.
[3] P. Cundall and O. D. L. Strack. A discrete numerical model for granular assemblies. *Géotechnique*, vol. 29, n. 1, pp. 47–65, 1979.
[4] E. Campello. *Um modelo computacional para o estudo de materiais granulares*. PhD thesis, Escola Politécnica da Universidade de São Paulo, 2016.
[5] G. Cusatis and E. Ramyar. Discrete fresh concrete model for simulation of ordinary, self-consolidating, and printable concrete flow. *Journal of Engineering Mechanics*, vol. 148, 2021.
[6] E. Campello. A description of rotations for dem models of particle systems. *Computational Particle Mechanics*, vol. 2, pp. 109–125, 2015.
[7] E. Campello. A computational model for the simulation of dry granular materials. *International Journal of Non-Linear Mechanics*, vol. 106, pp. 89–107, 2018.
[8] O. D. Quintana-Ruiz and E. M. Campello. Discrete element modeling of selective laser sintering additive manufacturing processes. *Computer Methods in Applied Mechanics and Engineering*, vol. 410, pp. 115994, 2023.